Multiphoton imaging microscopy at deeper layers with adaptive optics control of spherical aberration

Juan M. Bueno
Martin Skorsetz
Raquel Palacios
Emilio J. Gualda
Pablo Artal

Multiphoton imaging microscopy at deeper layers with adaptive optics control of spherical aberration

Juan M. Bueno, Martin Skorsetz, Raquel Palacios, Emilio J. Gualda, and Pablo Artal
Universidad de Murcia, Instituto Universitario de Investigación en Óptica y Nanofísica, Laboratorio de Óptica, Campus de Espianrdo (Ed. 34), 30100 Murcia, Spain

Abstract. Despite the inherent confocality and optical sectioning capabilities of multiphoton microscopy, three-dimensional (3-D) imaging of thick samples is limited by the specimen-induced aberrations. The combination of immersion objectives and sensorless adaptive optics (AO) techniques has been suggested to overcome this difficulty. However, a complex plane-by-plane correction of aberrations is required, and its performance depends on a set of image-based merit functions. We propose here an alternative approach to increase penetration depth in 3-D multiphoton microscopy imaging. It is based on the manipulation of the spherical aberration (SA) of the incident beam with an AO device while performing fast tomographic multiphoton imaging. When inducing SA, the image quality at best focus is reduced; however, better quality images are obtained from deeper planes within the sample. This is a compromise that enables registration of improved 3-D multiphoton images using nonimmersion objectives. Examples on ocular tissues and nonbiological samples providing different types of nonlinear signal are presented. The implementation of this technique in a future clinical instrument might provide a better visualization of corneal structures in living eyes. © *2014 Society of Photo-Optical Instrumentation Engineers (SPIE)* [DOI: 10.1117/1.JBO.19.1.011007]

Keywords: multiphoton microscopy; wavefront aberration; adaptive optics; human ocular tissue.

Paper 130161SSR received Mar. 20, 2013; revised manuscript received May 27, 2013; accepted for publication Jun. 11, 2013; published online Jul. 17, 2013.

1 Introduction

Two-photon excitation fluorescence (TPEF)[1] and second-harmonic generation (SHG) imaging[2] are forms of nonlinear microscopy being used in all major areas of biomedical research. Although these techniques allow intrinsic optical sectioning and three-dimensional (3-D) imaging, aberrations caused by the alignment and quality of the optical elements, the objective-sample refractive-index mismatch, and the inhomogeneous structure of the sample[3–7] limit their performance.[3] These enlarge, both laterally and axially, the focal spot within the specimen and reduce the multiphoton excitation efficiency, which leads to a reduction in the quality of the images.

In the last decade adaptive optics (AO) yielded substantial improvements in the images obtained with multiphoton microscopy.[3–6,8–11] In an ideal situation, for each location within the sample, the corresponding wavefront should be accurately measured and corrected. However, since the plane-by-plane wavefront assessment may be complex in thick samples, most of the authors used sensorless techniques for aberration correction.[3–6] Strategies are based on different algorithms modifying the incoming wavefront to improve the recorded image according to different quality metrics, such as intensity, contrast, or sharpness.[6,12]

These experiments provided image quality improvements by means of an indirect measurement of the actual aberrations within the sample. Only a few studies combined wavefront sensing and correction in multiphoton microscopy.[8–11]

It is well known that the use of a high numerical aperture (NA) objective induces spherical aberration (SA) due to the refractive-index mismatch at the interface between materials.[13,14] When a microscope is focused into the specimen, SA is induced, leading to a degradation of the images of deeper layers. Then, SA plays an important role when imaging thick samples with a multiphoton microscope. Moreover, it has been reported that SA is often the dominant term[3,4,6,15,16] and its correction leads to image enhancement.

Methods to correct for (or minimize) this unwanted SA in multiphoton microscopy were mainly based on the use of an objective correction collar[15,16] or a sensorless AO device.[3–6] For these experiments high-NA immersion objectives and previously chosen cover glasses (to minimize the refractive-index mismatch and the SA produced at the corresponding interface) are often used. The correction collar is a manual method only valid for a well-defined set of cover thickness values. An optimal performance depends on the relationship between the refractive indices of the immersion medium and the sample, and how uniform the refractive index within the specimen is.[15]

Alternatively, sensorless schemes offer a different strategy to compensate for different aberration terms by indirect assessment.[3–6] AO multiphoton microscopes based on modal Zernike correction[12] have reported interesting results. However, the effects of partial correction or induction of pure aberrations terms have not been studied in detail. In particular, SA increases imaging depth (i.e., induces a larger depth of focus), a feature that can be used in 3-D microscopy. Therefore, it is conceivable that the manipulation of the wavefront aberrations of the incident laser beam (via AO) to induce predefined values of SA may help to optimize multiphoton signals from deeper

Address all correspondence to: Juan M. Bueno, Universidad de Murcia, Instituto Universitario de Investigación en Óptica y Nanofísica, Laboratorio de Óptica, Campus de Espianrdo (Ed. 34), 30100 Murcia, Spain. Tel: +34 868888335; Fax: +34 868883528; E-mail: bueno@um.es

layers. In this sense, the aim of this study is to further analyze the influence of the SA on 3-D multiphoton imaging and in particular the effect in imaging deeper sample layers. We will examine the possibility of using a nonimmersion objective and an AO module to optimize both TPEF and SHG imaging in nonbiological samples and ocular tissues.

2 Experimental Setup and Procedure

2.1 Adaptive Optics Multiphoton Microscope

The experimental setup (Fig. 1) combines an AO module and a research prototype multiphoton microscope.[9] A 76-MHz, 110-fs Ti:sapphire mode-locked laser system (Mira900f, Coherent, St. Clara, CA) centered at 760 nm was used for the multiphoton excitation. This was coupled into an inverted microscope (Nikon TE2000-U, Tokyo, Japan). A pair of nonresonant galvanometric mirrors (GSI, VM1000, Billerica, MA) together with a Z-axis step motor (PI C-136, Karlsruhe, Germany) allowed the acquisition of XY images at different depths within the sample under study. A Plan Fluor $20 \times /0.5$ NA air long-working distance microscope objective (WD 2.1, Nikon ELWD Series) was used for the experiments described herein. Nonlinear signals (both TPEF and SHG) were collected via the same objective (backscattering configuration). A dichroic mirror separated these nonlinear backscattered signals from the infrared light used for multiphoton excitation. These signals emitted by the sample passed a spectral filter and reached the photomultiplier tube. Spectral filters in the detection channel were used to isolate either TPEF (broadband fluorescence filter, FGL435, Thorlabs Inc., Newton, NJ) or SHG (narrow-band spectral filter, 380 ± 10 nm; FB380-10, Thorlabs Inc.) signals. Image recording was completely controlled through a custom LabView™ (Austin, TX) interface. Image post-processing was performed with MATLAB™ (The MathWorks, Inc., Natick, MA). A continuously variable neutral density filter (not shown in Fig. 1) placed in front of the laser was used to set the appropriate average illumination power at the sample's plane.

2.2 Closed-Loop Wavefront Aberration Control

The AO module, composed of a Hartmann–Shack (HS) wavefront sensor and a deformable mirror (DM),[9] was used to control
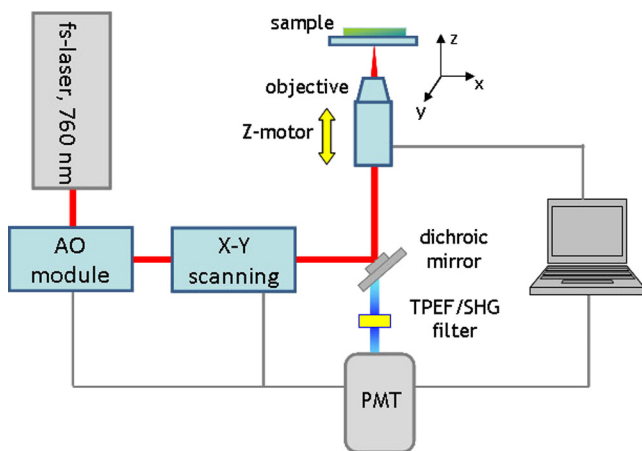

Fig. 1 Schematic diagram of the adaptive optics (AO) multiphoton microscope. The AO module is composed of a Hartmann–Shack wavefront sensor and a deformable mirror; PMT, photomultiplier tube.

and manipulate the laser beam aberrations while multiphoton microscopy was performed. The AO module was calibrated in a previous operation. The high-power laser beam passed through this AO module before entering the microscope (see Fig. 1). The corrector device was a gold-coated MEMS-type 140-actuator DM (Boston Micromachines, Cambridge, MA). The HS sensor (WFS150-5C, Thorlabs Inc.) measured the laser beam aberrations and those induced by the DM, and working in closed loop, the AO module set the target wavefront, expressed as a Zernike polynomial expansion. By setting the appropriate DM shape, the system was able to reach a final wavefront composed of any possible combination of Zernike modes (the limit is imposed by the DM stroke). In this experiment, the AO module has been used to produce predefined values for the SA (Z_4^0) correcting for the rest of the aberration modes. To achieve this, initially the AO system measured the beam's wavefront and set these values to the target aberration, except for the SA whose value was previously stated as desired.

The experimental system was first set to sequentially record multiphoton XZ tomographic (cross-sectional) images[17] for different amounts of SA induced by the AO module. SA values were produced in steps of 0.05 μm. This imaging modality permits a fast transversal visualization of the sample (a few seconds). From each tomography the averaged intensity profile as a function of depth was automatically computed. The image with the highest area under the intensity profile was considered to provide the most appropriate SA value for the sample under study. This procedure was carried out for each sample involved in the study.

Once this "optimum" SA value was determined, two stacks of regular XY multiphoton images at different depth locations were recorded, with and without inducing this SA value. Moreover, to establish the relative impact of this optimum SA in the multiphoton microscopy images, different image quality parameters were also computed.[18] Moreover, for each parameter P a relative improvement (in %) was defined as follows:

$$\text{improvement} = \frac{P_{\text{SA}} - P_{\text{SA}=0}}{P_{\text{SA}=0}} \times 100, \qquad (1)$$

with P being the values of the corresponding parameter in the images obtained with a given value of SA and without SA (SA = 0).

2.3 Samples

In order to test the feasibility of the procedure reported herein, different samples were used in the experiment. As nonbiological samples, a piece of cellulose and grains of starch sample were used. These provide TPEF and SHG signals.[9] As biological specimens, we used human epiretinal membranes, chicken retinal tissue, and porcine corneas. The corneal stroma (made of type I collagen),[19–21] produces SHG signal and retinal tissues provide a remarkable TPEF signal.[22–24] Chicken retinas and human epiretinal membranes were flat-mounted on a microscope slide after overnight fixation with a paraformaldehyde solution (additional details can be found in Ref. 24). Porcine eyes were obtained from a local slaughterhouse (refer to Ref. 21 for further details on the manipulation). These intact ocular globes were placed upside-down on a glass-bottom dish for multiphoton microscopy imaging.
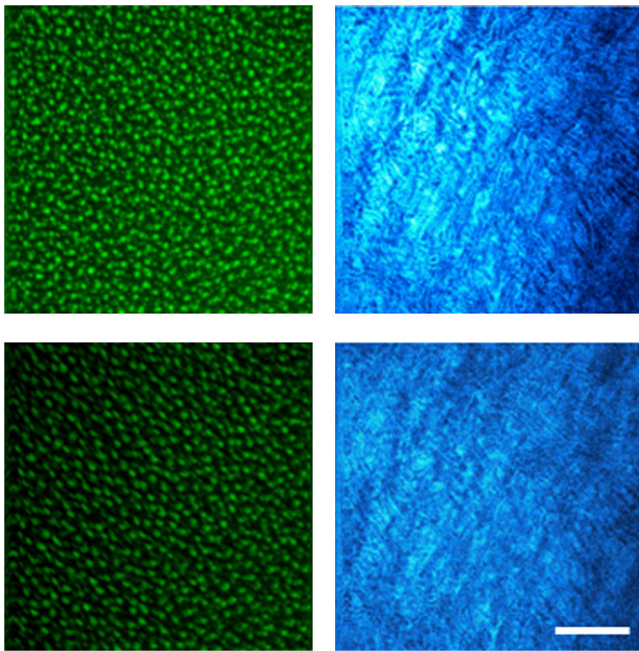
Fig. 2 Effects of SA on multiphoton images. Top row images (SA = 0 μm) must be compared to those of the bottom row (SA = +0.1 μm). Samples correspond to chicken retina (left) and porcine cornea (right). False color has been used for a better understanding: green for TPEF and blue for SHG. Imaged single planes correspond to the best focus within the sample. Bar length: 50 μm.

Fig. 4 (a) Comparison of tomographic TPEF images of a single cellulose fiber for different values of induced SA (0 μm, left; −0.1 μm, center; −0.2 μm, right). (b) Intensity profiles as a function of depth, when inducing different controlled amounts of SA compared to the case of complete aberration correction (black line).

3 Results

3.1 Effect of Aberration Correction on Single Plane Images

The influence of SA was first tested by recording individual planes of different samples as shown in Fig. 2. A direct comparison can be made for retinal and corneal tissues providing TPEF (left panels, photoreceptors mosaic) and SHG (right panels, stroma collagen fibers) signals, respectively. As expected, the addition of 0.1 μm of SA led to a reduction in the image quality for both specimens (bottom panels). All image quality metrics (total intensity, entropy, signal-to-noise ratio) reduced when inducing SA (between 8% and 40% depending on the metric).

Another preliminary experiment on the dominance of SA over other aberration terms was also carried out. As an example Fig. 3 includes TPEF images of a plane located 100 μm inside a piece of cellulose. The impact of using just SA [Fig. 3(b)] or also

other terms such as astigmatism and coma [Fig. 3(c)] can be directly compared to a control image [no AO module in use, Fig. 3(a)]. This illustrative example confirms the dominance of the SA and helps to understand our choice of SA as a unique term to improve multiphoton imaging in thick samples.

3.2 Effect of Spherical Aberration on Depth Imaging

Tomographic images of the samples for different amounts of SA were first acquired [see an example of these images in Fig. 4(a)]. As explained in Sec. 2, for each tomographic image (and SA value) the averaged intensity profile was computed. Figure 4(b) shows the impact of inducing different controlled amounts of SA as a function of the sample's depth compared to the case of complete aberration correction.

When SA was not induced, the TPEF signal decreased with depth because of the influence of the specimen aberrations themselves [black line in Fig. 4(b)]. The intensity values reduced at the best imaged plane when SA was induced: the higher the SA the more reduction. For SA = −0.1 μm the intensity was below the optimal one and provided similar values for deeper locations, as seen by comparing black and black dashed lines. However, this behavior clearly changed when adding larger values of SA. For this sample, this occurred when SA
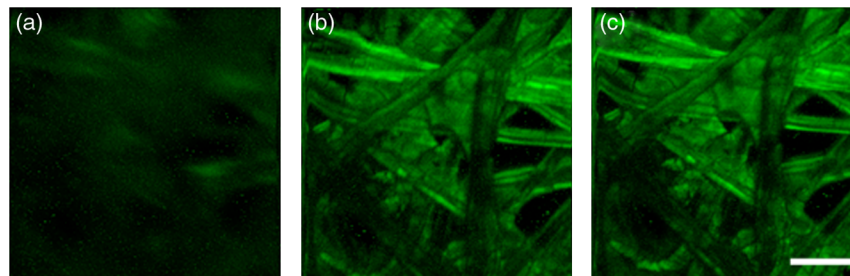

Fig. 3 Impact of SA and other aberration terms on TPEF image quality. (a) Image control; (b) SA; (c) SA, astigmatism, and coma. All images have the same intensity scale. Bar length: 50 μm.

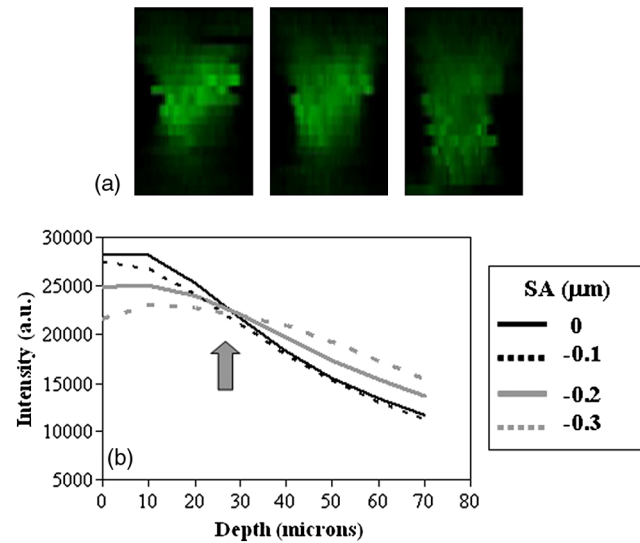was larger than −0.15 μm (gray lines). The arrow in the plot indicates the location where the behavior was reversed, i.e., a better TPEF signal was obtained when imaging deeper into the sample. This implies an extended imaging depth (or alternatively an increase in the depth of focus) from deeper positions within the sample. It is also interesting to observe that for SA = −0.3 μm (and larger values not shown here) the effects are more noticeable for deeper planes, although a shift in the optimal focal plane is also produced.

From the intensity profiles the optimum SA value was determined (see Sec. 2) and 3-D multiphoton imaging immediately performed (i.e., *XY* images along the *Z* direction). These stacks of images for different depth positions were recorded for two experimental conditions: with the optimum SA value and without SA (for comparison purposes). This 3-D imaging gives us information on the interaction between SA and the quality of images from deeper planes. Figure 5 presents an example of TPEF images at different depth locations for the two experimental conditions: SA = 0 μm (top row) and SA = −0.2 μm. The improvement of images at planes located 50 and 75 μm within the sample can be qualitatively observed.

For a better understanding of this SA impact, Fig. 6(a) presents the corresponding total intensity values (across the entire images) as a function of depth. The tendency for the rest of the image quality metrics (not shown here) was also similar. Moreover, although different image quality metrics are expected to measure different image properties,[18] the reversal point positions (see arrow) hardly differ among the different metrics (not more than 3 μm for the samples here used). Figure 6(b) presents the improvement in total TPEF signal versus depth position. This becomes positive when the effect the SA is reversed. Similar results are obtained for a human epiretinal membrane also providing TPEF signal. Results are depicted in Fig. 7.

For completeness, the procedure was also applied to samples providing SHG signal. The increase in depth imaging for a sample of starch grains is also evident for two different metrics (total intensity and entropy) as depicted in Fig. 8. For this sample, a value of −0.1 μm SA was the optimal value to observe the improvement.

Finally, the procedure was also applied to another biological sample: porcine corneal tissue providing SHG signal originated
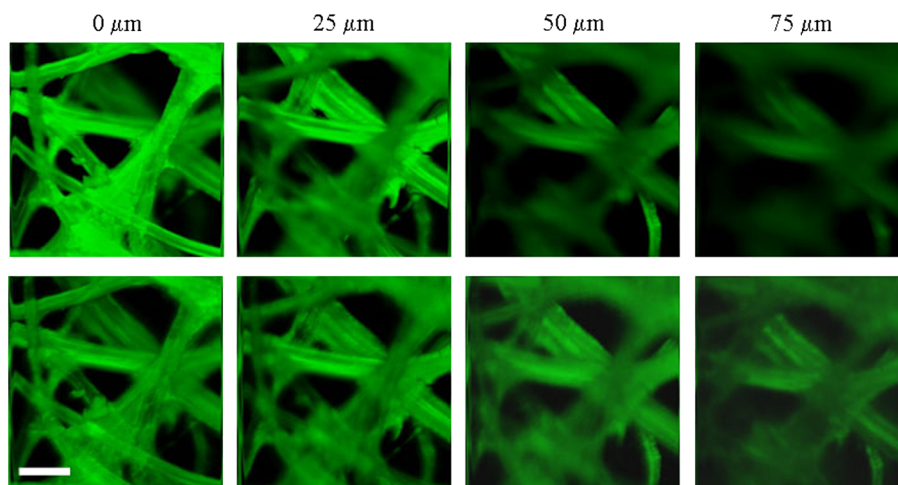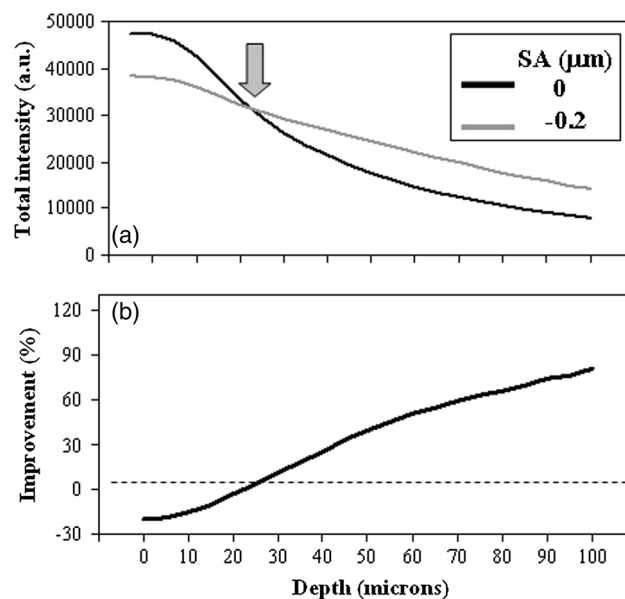

Fig. 6 (a) Effect of inducing −0.2 μm SA (gray line) compared to the case of null SA (black line). (b) Improvement in the total TPEF intensity of the images as a function of depth.

at the stroma. It is known that within the cornea, the deeper the image plane is located, the lower the SHG signal recorded,[25] as upper panels of Fig. 9 show. However, when the illumination laser beam contains a certain amount of SA (bottom panels of Fig. 9), beyond a particular depth location the intensity levels do not follow that behavior. For this particular sample, −0.1 μm SA was the optimal value to observe the effect analyzed in this work. In Fig. 10, this improvement in SHG signal as a function of depth is depicted.

4 Discussion

During the last decade, there has been a remarkable interest in the development of novel AO capabilities for improved 3-D high-resolution multiphoton microscopy imaging. Most reported techniques are sensorless and improved the focal spot within the sample by pre-shaping the wavefront of the input
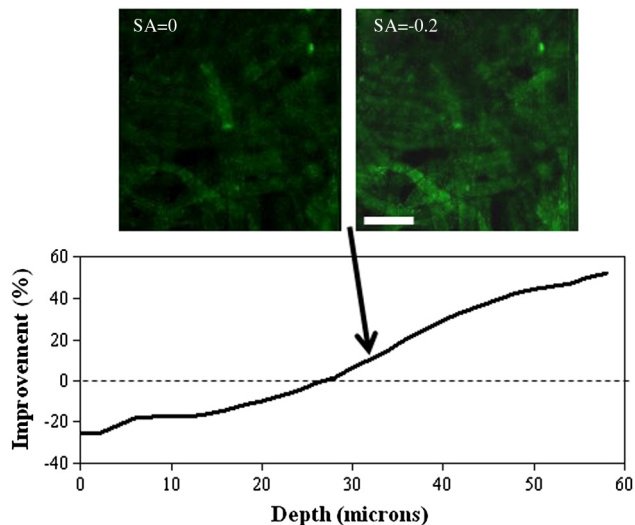

Fig. 5 TPEF images for different depth positions acquired with all laser beam aberrations corrected (top row) and −0.2 μm SA induced (optimum value for this sample). The sample corresponds to a piece of cellulose. Bar length: 50 μm.

Fig. 7 Improvement in TPEF signal as a function of depth for a human epiretinal membrane when inducing −0.2 μm SA compared to the case of complete aberration correction. The arrow indicates the depth location of the images within the sample. Bar length: 50 μm.
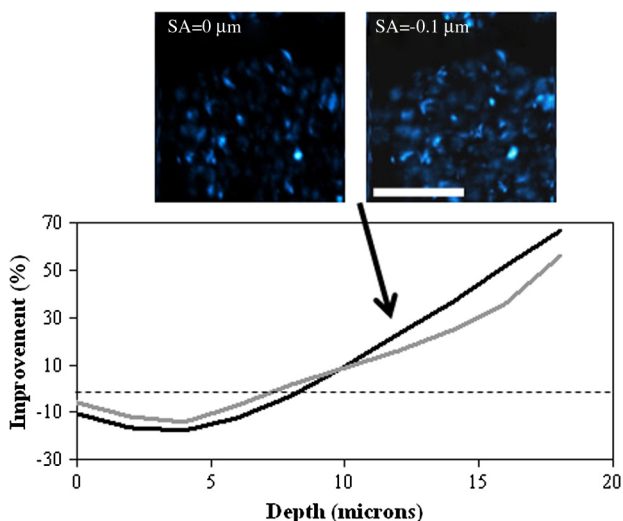

Fig. 8 SHG signal improvement measured with total intensity (black line) and entropy (gray line) as a function of depth when inducing −0.1 μm SA. The arrow indicates a depth location of 12 μm. The sample corresponds to starch grains. Bar length: 50 μm.

beam to compensate for the specimen-induced aberration according to a sequential adjust of individual Zernike modes.[6]

In this sense, this study has reported that an accurate manipulation of the aberrations in the illuminating beam provides improved 3-D multiphoton imaging. The AO module has not been used for a modal plane-to-plane correction, but to induce controlled amounts of SA, working in closed loop. This manipulation of the incident laser beam aberrations leads to an improvement in the nonlinear signal from images (as measured with different metrics) acquired at deeper locations within the sample. This effect might be understood as increased imaging depth or extended depth of focus and has been demonstrated in non-biological and biological (ocular tissues) samples providing both TPEF and SHG signals.

For each sample, the appropriate SA value was computed from fast tomographic nonlinear imaging (for this experiment the highest induced SA value was −0.3 μm, in steps of 0.05 μm). This value corresponds to the image with the highest area under the intensity profile. With this optimum induced SA, each sample was imaged with depth in a regular manner ($XY + Z$ scanning). Although the required SA values were particular for each sample, they were never larger than −0.2 μm here. The percent of improvement at a certain depth location depended also on the used sample. The shallowest plane at which this improvement takes place was ∼7 μm for starch. For the rest of the samples, it was placed between 25 and 30 μm.

The effects of SA in both linear (bright-field and confocal) and nonlinear microscopy have been a topic of interest.[4,15,16,26–28] Implementations to eliminate or minimize the effect of SA in the former include an objective correction ring,[13,15,16] changes in the effective tube length of the microscope objective,[28,29] structured illumination techniques,[30,31] point-spread function engineering,[32] and AO devices,[6,33–35] among others.

Although to minimize SA some objectives have a correction ring to adjust for the thickness of the microscope slide, additional SA is also present when focusing deeper within the specimen. Moreover, when imaging specimens in a backscattered configuration, the main drawback is the noticeable reduction of the signal for deeper planes. The anterior layers will produce aberrations that might interfere with the measurement from deeper layers as the light travels through. Lo and coworkers analyzed the effects of a collar in multiphoton microscopy of tendon and skin (maximum depth: 28 μm).[15] Although their results showed some improvements, they ignored the nominal SA values required for each sample and depth. They also claimed that the collar's ability to compensate for the SA decreased with depth and that the required correction collar settings were particular for each sample and distribution of refraction indices. Muriello and Dunn reported a similar experiment.[16] The combination of a water immersion objective lens and a correction collar decreased the depth dependence of signal levels in TPEF images of kidney tissue. Débarre et al. combined an immersion objective collar and a DM to pre-compensate for different aberration terms (SA included) in a mouse embryo.[6] This procedure is robust but highly time-consuming (minutes).

Despite that aberrations are specimen-dependent, these tend to be dominated by a small number of low-order Zernike aberration modes. The magnitude of the aberrations increases with NA.[36,37] Although the ideal compensation would require a plane-by-plane SA correction, in the present work, we have demonstrated that this is not always necessary. We report that an appropriate value of SA can experimentally be measured for each sample in order to improve the image quality of deeper planes because the depth of focus is extended. This procedure, although with some limitations, represents a more elegant and accurate method than an objective collar, where the effect is limited by the discrete values provided by the collar itself.

Unlike most experiments reported in the literature (using immersion high-NA objectives), the objective here used is a low-NA air long-working distance objective. These "air-immersion" objectives would be more suitable for future *in vivo* experiments. In this sense, the SA value produced in the illumination beam has a double function: (1) a basal correction compensating for the refractive-index mismatch air-microscope cover and (2) an additional correction to partially compensate for the specimen-induced SA. The reduction of image quality
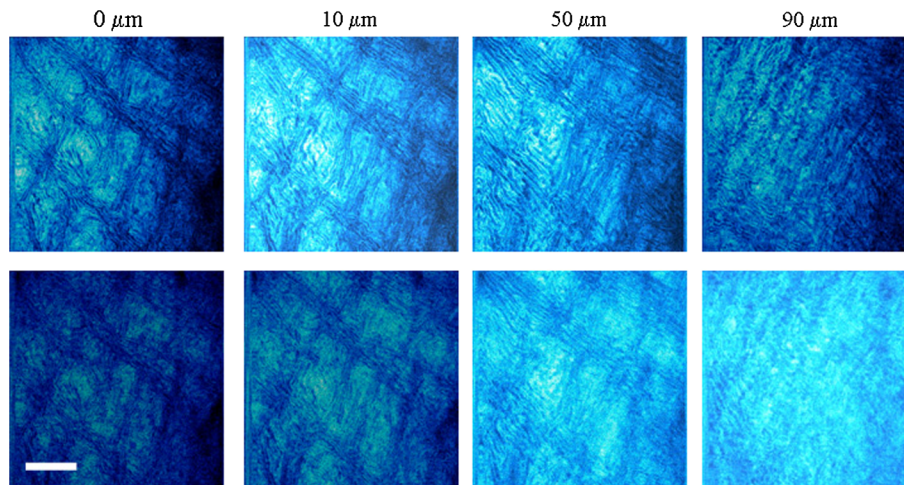
Fig. 9 SHG imaging of corneal stroma at different depth locations illustrating the effects of adding −0.1 μm SA to the illumination laser beam (bottom panels). Upper panels correspond to the case of all laser beam aberrations corrected. The sample is an *ex vivo* porcine cornea. Bar length: 50 μm.

is affected by SA to a large extent.[36] Despite that the rest of aberration terms are not corrected and a unique value (experimentally computed) of SA is used, the image quality is improved.

Compared to the experimental conditions using a total laser beam aberration correction,[9] the "side-effect" of the proposed technique is that the signal at the best imaged plane of the sample is reduced. However, for deeper planes the behavior is reversed, the signal is improved, and more details are visible. Although the enhancement depends on each particular sample, the extended imaging depth has been demonstrated for both TPEF and SHG signals. Moreover, the procedure here reported overpasses (to some extent) the limitation of a single aberration correction per depth (since a unique customized aberration is used) which significantly decreases scan times and enables more rapid imaging. The approach reported in this paper provides a fine balance on the effect of SA aberrations in stacks of nonlinear images. While SA reduces the image quality at best focus, it provides a better series of images at deeper layers. If the amount of incoming light can be easily selected, this can be a better compromise providing a range of improved images.

The present procedure is much faster than a possible plane-by-plane correction. The typical acquisition time for tomography imaging modality is about 5 s for a 100-μm-thick sample (at 3 μm Z-step). The sequential use of six SA values with the computation of the intensity profiles took approximately 40 s.

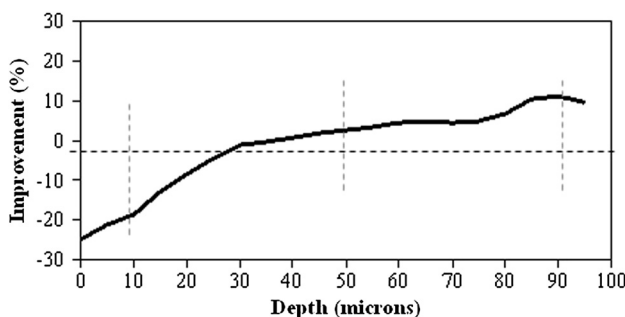**Fig. 10** Improvement in the SHG intensity of corneal stroma images as a function of depth when inducing −0.1 μm SA. Vertical dotted lines correspond to the locations of images in Fig. 9.

Once the SA value has been determined, the regular XY imaging (planes taken 5 μm apart) will take ∼1 min. The images for a plane-by-plane correction provide better quality, but the time used is much longer. In particular, with our experimental configuration, >5 min would necessary to complete the entire operation.

A plane-to-plane correction provides a more accurate SA correction, but the time required for it is excessively long when living samples are imaged. In this sense, the main advantage of our procedure is that it could be used to improve the imaging of living specimens such as embryos or brain neurons, among others.

Probably one of the most interesting consequences is provided by results in Fig. 10. The imaging of corneal tissue in living animals (human included) is a challenging application. Fast recording procedures are of special interest for *in vivo* applications. The use of the present technique with a nonimmersion objective when imaging the living cornea would produce improved images while decreasing acquisition times, minimizing photobleaching effects, reducing tissues damage, and keeping the safety limits (strongly necessary in ophthalmology).

5 Conclusions

We have used an AO multiphoton microscope in a backscattered configuration and a nonimmersion low-NA objective to improve 3-D nonlinear imaging. The technique was based on an accurate aberration control of the illuminating beam. In particular, controlled amounts of SA led to an increase in imaging depth independently of the specimen-induced aberrations, which is essential in multiphoton microscopy. The benefits of this AO procedure have been tested in both nonbiological and biological samples, with particular interest in *ex vivo* ocular tissues. In this type of tissue, an extended imaging depth might be of huge interest to better visualize deep retinal and corneal layers through volume rendering reconstructions. The procedure here described partially overpasses the limits imposed by the aberrations, improves the multiphoton microscopy sectioning capabilities, and represents a further step to produce 3-D images with overall increased quality. This technique might be of great interest in future studies of living samples, especially clinical applications including corneal tissue imaging.

Acknowledgments

References

1. W. Denk, J. H. Strickler, and W. W. Webb, "Two-photon laser scanning fluorescence microscopy," *Science* **248**(4951), 73–76 (1990).
2. P. J. Campagnola et al., "Second-harmonic imaging microscopy of living cells," *J. Biomed. Opt.* **6**(3), 277–286 (2001).
3. L. Sherman et al., "Adaptive correction of depth-induced aberrations in multiphoton scanning microscopy using a deformable mirror," *J. Microsc.* **206**(1), 65–71 (2002).
4. M. A. Neil et al., "Adaptive aberration correction in a two-photon microscope," *J. Microsc.* **200**(2), 105–108 (2000).
5. P. N. Marsh, D. Burns, and J. M. Girkin, "Practical implementation of adaptive optics in multiphoton microscopy," *Opt. Express* **11**(10), 1123–1130 (2003).
6. D. Débarre et al., "Image-based adaptive optics for two-photon microscopy," *Opt. Lett.* **34**(16), 2495–2497 (2009).
7. J. M. Bueno et al., "Temporal wavefront stability of an ultrafast high-power laser beam," *Appl. Opt.* **48**(4), 770–777 (2009).
8. M. Rueckel, J. A. Mack-Bucher, and W. Denk, "Adaptive wavefront correction in two-photon microscopy using coherence-gated wavefront sensing," *Proc. Natl. Acad. Sci. U.S.A.* **103**(46), 17137–17142 (2006).
9. J. M. Bueno, E. J. Gualda, and P. Artal, "Adaptive optics multiphoton microscopy to study ex-vivo ocular tissues," *J. Biomed. Opt.* **15**(6), 066004 (2010).
10. J. W. Cha, J. Ballesta, and P. T. C. So, "Shack–Hartmann wavefront-sensor-based adaptive optics system for multiphoton microscopy," *J. Biomed. Opt.* **15**(4), 046022 (2010).
11. R. Aviles-Espinosa et al., "Measurement and correction of in vivo sample aberrations employing a nonlinear guide-star in two-photon excited fluorescence microscopy," *Biomed. Opt. Express* **2**(11), 3135–3149 (2011).
12. A. J. Wright et al., "Exploration of the optimisation algorithms used in the implementation of Adaptive Optics in confocal and multiphoton microscopy," *Microsc. Res. Tech.* **67**(1), 36–44 (2005).
13. M. J. Booth et al., "Adaptive aberration correction in a confocal microscope," *Proc. Natl. Acad. Sci. U.S.A.* **99**(9), 5788–5792 (2002).
14. M. J. Booth and T. Wilson, "Refractive-index-mismatch induced aberrations in single-photon and two-photon microscopy and the use of aberration correction," *J. Biomed. Opt.* **6**(3), 266–272 (2001).
15. W. Lo et al., "Spherical aberration correction in multiphoton fluorescence imaging using objective correction collar," *J. Biomed. Opt.* **10**(3), 034006 (2005).
16. P. A. Muriello and K. W. Dunn, "Improving signal levels in intravital multiphoton microscopy using an objective correction collar," *Opt. Commun.* **281**(7), 1806–1812 (2008).
17. J. M. Bueno et al., "Multiphoton microscopy of ex vivo corneas after collagen cross-linking," *Invest. Ophthalmol. Visual Sci.* **52**(8), 5325–5331 (2011).
18. J. M. Bueno et al., "Characterizing image quality in a scanning laser ophthalmoscope with differing pinholes and induced scattered light," *J. Opt. Soc. Am. A* **24**(5), 1284–1295 (2007).
19. M. Han, G. Giese, and J. Bille, "Second harmonic generation imaging of collagen fibrils in cornea and sclera," *Opt. Express* **13**(15), 5791–5797 (2005).
20. N. Morishige et al., "Noninvasive corneal stromal collagen imaging using two-photon-generated second-harmonic signals," *J. Cataract Refractive Surg.* **32**(11), 1784–1791 (2006).
21. J. M. Bueno, E. J. Gualda, and P. Artal, "Analysis of corneal stroma organization with wavefront optimized nonlinear microscopy," *Cornea* **30**(6), 692–701 (2011).
22. M. Han et al., "Two-photon excited autofluorescence imaging of human retinal pigment epithelial cells," *J. Biomed. Opt.* **11**(1), 010501 (2006).
23. J. M. Bueno et al., "Analysis of the chicken retina with an adaptive optics multiphoton microscope," *Biomed. Opt. Express* **2**(6), 1637–1648 (2011).
24. E. J. Gualda, J. M. Bueno, and P. Artal, "Wavefront optimized nonlinear microscopy of ex-vivo human retinas," *J. Biomed. Opt.* **15**(2), 026007 (2010).
25. J. M. Bueno, E. J. Gualda, and P. Artal, "Non-linear 3D microscopy of ex vivo corneas," *Proc. SPIE* **7569**, 756937 (2010).
26. C. J. R. Sheppard and T. Wilson, "Effect of spherical aberration on the imaging properties of scanning optical microscopes," *Appl. Opt.* **18**(7), 1058–1063 (1979).
27. P. Török, S. J. Hewlett, and P. Vargas, "The role of specimen-induced spherical aberration in confocal microscopy," *J. Micros.* **188**(2), 158–172 (1997).
28. S. Hell et al., "Aberration in confocal fluorescence microscopy induced by mismatches in refractive index," *J. Microsc.* **169**(3), 391–405 (1993).
29. C. J. R. Sheppard, "Aberrations in high aperture conventional and confocal imaging systems," *Appl. Opt.* **27**(22), 4782–4786 (1988).
30. M. A. A. Neil, R. Juskaitis, and T. Wilson, "Method of obtaining optical sectioning by using structured light in a conventional microscope," *Opt. Lett.* **22**(24), 1905–1907 (1997).
31. M. Arigovindan, J. W. Sedat, and D. A. Agard, "Effect of depth dependent spherical aberrations in 3D structured illumination microscopy," *Opt. Express* **20**(6), 6527–6541 (2012).
32. S. Yuan and C. Preza, "Point-spread function engineering to reduce the impact of spherical aberration on 3D computational fluorescence microscopy imaging," *Opt. Express* **19**(23), 23298–23314 (2011).
33. P. S. Tsai et al., "Spherical aberration correction in nonlinear microscopy and optical ablation using a transparent deformable membrane," *Appl. Phys. Lett.* **91**, 191102 (2007).
34. M. Shaw et al., "Characterization of deformable mirrors for spherical aberration correction in optical sectioning microscopy," *Opt. Express* **18**(7), 6900–6913 (2010).
35. D. Iwaniuk, P. Rastogi, and E. Hack, "Correcting spherical aberrations induced by an unknown medium through determination of its refractive index and thickness," *Opt. Express* **19**(20), 19407–19414 (2011).
36. M. J. Booth, M. A. A. Neil, and T. Wilson, "Aberration correction for confocal imaging in refractive-index-mismatched media," *J. Microsc.* **192**(2), 90–98 (1998).
37. M. Schwertner et al., "Measurement of specimen-induced aberrations of biological samples using phase stepping interferometry," *J. Microsc.* **213**(1), 11–19 (2004).